Thermochimica Acta 605 (2015) 16–21

Contents lists available at ScienceDirect

Thermochimica Acta

journal homepage: www.elsevier.com/locate/tca

Precursor combustion synthesis of nanocrystalline cobalt substituted nickel zinc ferrites from hydrazinated mixed metal fumarates

S.G. Gawas, V.M.S. Verenkar *

Department of Chemistry, Goa University, Taliegao Plateau, Goa 403206, India

ARTICLE INFO

Article history:
Received 15 November 2014
Received in revised form 19 January 2015
Accepted 12 February 2015
Available online 14 February 2015

Keywords:
Hydrazinated precursor
Exothermic
Autocatalytic decomposition
Nanocrystalline
Ni–Zn ferrites

ABSTRACT

In present investigation, a systematic approach towards synthesis of nanocrystalline ferrites, $Co_xNi_{0.6-x}Zn_{0.4}Fe_2O_4$ ($x = 0.1$ and 0.4) has been reported by room temperature decomposition of precursors, $Co_xNi_{0.6-x}Zn_{0.4}Fe_2$ $(C_4H_2O_4)_3{\cdot}6N_2H_4$ ($x = 0.1$ and 0.4). The precursor complexes were characterized by Fourier transform infrared spectroscopy (FTIR), chemical analysis and thermal studies like isothermal mass loss, total mass loss, thermogravimetry (TG), derivative of thermogravimetry (DTG) and differential thermal analysis (DTA). The TG–DTG–DTA patterns of both precursors reveal multistep decomposition with complete ferritization at 410 °C. The thermally decomposed products were characterized by X-ray diffractometry (XRD) for phase purity. The FT-IR spectroscopy studies of the same shows complete removal of all organic moieties from decomposed precursors. The nanophasic nature of synthesized ferrites was confirmed by transmission electron microscopy (TEM) analysis as well as from broadening of XRD peaks. The AC magnetization studies show the existence of single domain and superparamagnetic particles, which supports nanosize particles distribution in the ferrite system under study.

1. Introduction

The research in synthesis of nanocrystalline materials with desired geometry, size and stoichiometry is increasing day by day due to different properties they show than the bulk. Actually, the composition, cation distribution and particle size and shape are the important factors responsible for deviation in structural and magnetic properties [1–4] thereby opening doors of newer applications in various areas of interest such as sensing of toxic gases, medical field and in catalysis as magnetically recoverable catalyst for organic transformation [5–8]. Materials, especially magnetic ferrites are gaining attention of research groups from different fields due to their application from nanometric scale to bulk. Ferrites are known to posses high resistivity and low eddy current loss which suites their candidature for higher frequency applications [9,10]. The hunger for achieving desired characteristics in ferrites has led to development of new synthetic strategies as well as improvement in the existing ones. Various instrumental and traditional wet chemical methods namely; combustion [11], sol-gel [12–14], coprecipitation [15,16], spray pyrolysis [17], hydrothermal synthesis [18], reverse micelle [19,20] and precursor [21–47] have been successfully employed for synthesis of nanocrystalline ferrites with compositional control and size uniformity. Among these methods, the precursor method is extensively explored by using different carboxylates like citrates [21], malates [22], oxalates [23,24] etc., which involves decomposing of metal carboxylates in furnace above 400 °C to form nanocrystalline ferrite powder. Moreover some metal carboxylate precursors, coordinated with hydrazine has been found to undergo low temperature decomposition to metal oxides [25–49]. The present study describes systematic investigation towards synthesis of one such precursor namely, hydrazinated mixed metal fumarate and its decomposition to corresponding nanocrystalline ferrites and also the role of hydrazine in auto-decomposition of precursors.

2. Experimental

2.1. Synthesis

The hydrazinated mixed metal fumarates were synthesized by adding aqueous mixture of metal chlorides to sodium fumarate–hydrazine hydrate mixture, stirred for 2 h in N_2 atmosphere. The requisite amount of all the metal chloride mixture (except ferrous chloride) was prepared in aqueous medium while ferrous chloride solution was prepared fresh from iron powder and conc. HCl under CO_2 atmosphere. The analytical grade chemicals were used for synthesis. The yellow precipitate formed was filtered, washed with ethanol and dried with diethyl ether under suction. The above

* Corresponding author. Tel.: +91 832 6519321; fax: +91 832 2452886.
E-mail address: vmsv@rediffmail.com (V.M.S. Verenkar).

http://dx.doi.org/10.1016/j.tca.2015.02.010
0040-6031/

Table 1
Metal content and hydrazine analysis of $Co_xNi_{0.6-x}Zn_{0.4}Fe_2(C_4H_2O_4)_3{\cdot}6N_2H_4$ ($x = 0.1$ and 0.4).

Composition x	Mass%									
	Nickel		Cobalt		Zinc		Iron		Hydrazine	
	Obs.	Calc.	Obs.	Calc.	Obs.	Calc.	Obs.	Calc.	Obs.	Calc.
0.1	4.22	4.15	0.82	0.83	3.66	3.69	15.63	15.79	27.24	27.15
0.4	1.52	1.66	3.18	3.33	3.66	3.70	15.63	15.79	27.56	27.15

procedure was repeated to precipitate both the complexes and can be represented as follow.

$$MCl_{2(aq)} + 2FeCl_{2(aq)} + 3Na_2C_4H_2O_{4(aq)} + 6N_2H_4{\cdot}H_2O(aq) \rightarrow MFe_2(C_4H_2O_4)_3{\cdot}6N_2H_{4(S)} + 6NaCl_{(aq)} + 6H_2O_{(l)}\ (M = Co^{2+},\ Ni^{2+}, Zn^{2+})$$

2.2. Characterization

The hydrazinated mixed metal fumarate complexes were analyzed for their stoichiometry based on standard methods of analysis. The FT-IR studies of the precursors and their decomposed end products were carried out on a FTIR Shimadzu IR Prestigue-21 Spectrophotometer, to confirm the presence of different organic moieties and their linkage with metal ions in the complexes. The hydrazine content was chemically analyzed by volumetric analysis using 0.025 M KIO_3 as titrant under Andrew's condition [50]. Different metal content in precursor complexes were determined by titrating with EDTA, after decomposing the known amount of precursor in concentrated HCl followed by separation on column [50,51]. The simultaneous thermogravimetric (TG), derivative of thermogravimetry (DTG) and differential thermal analysis (DTA) measurements of the precursor were recorded from RT to 810 °C on a NETZSCH STA 409 PC (Luxx) analyzer. The experiments were carried out in dry air at a purge rate of 60 mL per min and ramping rate of 10 °C per min with 10-15 mg of the samples in alumina cups. The isothermal mass loss and total mass loss studies of the precursors were also carried out at different pre-determined temperature based on TG-DTA results. The structure and phase purity of the thermally decomposed end product of the precursors were studied using Rigaku Mini flex X-ray diffractometer with monochromatized Cu Kα radiation filtered through Ni absorber. The morphology was studied by transmission electron microscopy, taken from Philip's-CM20 electron microscope. The AC susceptibility measurements were carried out on DOSE AC susceptibility Setup standardized with Nickel, operating at 5000Oe and supplied by ADEC Embedded Technology and Solutions Pvt., Ltd., Corlim, Goa.

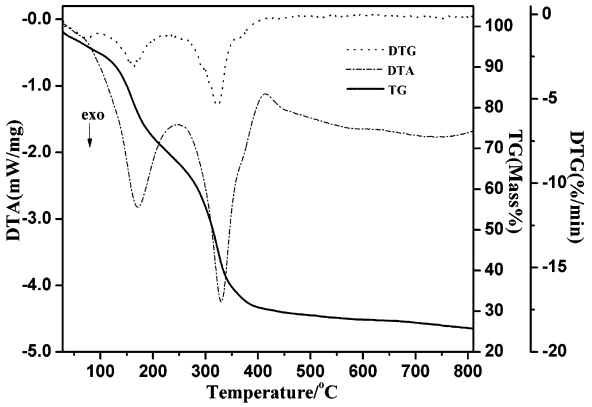

Fig. 2. TG–DTG–DTA plot of $Co_{0.1}Ni_{0.5}Zn_{0.4}Fe_2(C_4H_2O_4)_3{\cdot}6N_2H_4$.

2.3. Thermal decomposition of the hydrazinated fumarate precursors

The precursor complexes were uniformly spread in a ceramic clay dish and lighted with burning splinter. The precursor catches fire and a red glow that subsequently formed spreads immediately over the entire bulk to give auto-combusted nano-sized particles of $Co_xNi_{0.6-x}Zn_{0.4}Fe_2O_4$. These $Co_xNi_{0.6-x}Zn_{0.4}Fe_2O_4$ powders were further heated in air in a furnace at 450 °C for 5 h to remove any residual carbon formed during the decomposition of complexes and termed as "as prepared" ferrites in the following text.

3. Results and discussion

3.1. Chemical analysis and FTIR studies

The percentage content of different metals and hydrazine in precursors has been tabulated in Table 1. The stoichiometry has been assigned as, $Co_xNi_{0.6-x}Zn_{0.4}Fe_2(C_4H_2O_4)_3{\cdot}6N_2H_4$ ($x = 0.1$ and 0.4) based on the observed percentage of hydrazine, cobalt, nickel, zinc and iron which matches closely with the calculated values. The FTIR spectrums of both precursor complexes (Fig. 1) are identical and almost superimposable. Complexes show four bands in the region 3190–3353 cm^{-1} which are characteristic of N—H stretching frequencies. The observed N—N stretching frequencies

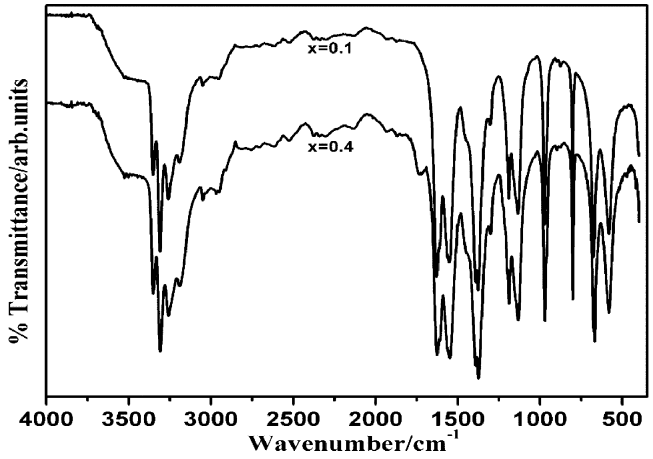

Fig. 1. FTIR spectra of $Co_xNi_{0.6-x}Zn_{0.4}Fe_2(C_4H_2O_4)_3{\cdot}6N_2H_4$ ($x = 0.1$ and 0.4).

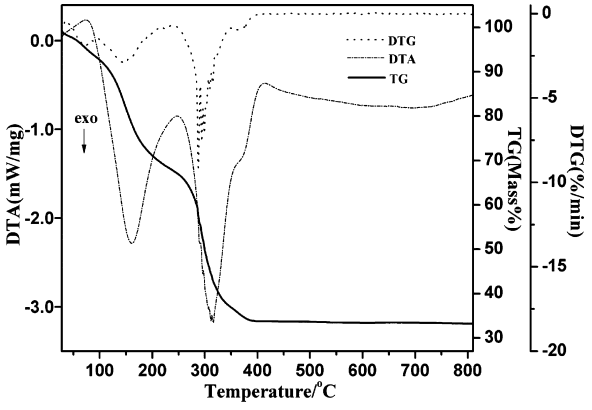

Fig. 3. TG–DTG–DTA plot of $Co_{0.4}Ni_{0.2}Zn_{0.4}Fe_2(C_4H_2O_4)_3{\cdot}6N_2H_4$.

Table 2
TG–DTA data of $Co_xNi_{0.6-x}Zn_{0.4}Fe_2(C_4H_2O_4)_3{\cdot}6N_2H_4$ ($x = 0.1$ and 0.4).

$x = 0.1$			$x = 0.4$			Remarks
TG		DTA	TG		DTA	
Temp. range (°C)	Mass loss (%)	Peak (°C)	Temp. range (°C)	Mass loss (%)	Peak (°C)	
RT-100	6.76	–	RT-100	7.12	74.5 (endo)	Loss of adsorbed hydrazine and/or moisture followed by total dehydrazination and beginning of decarboxylation
100–220	23.16	171.6 (exo)	100–220	23.58	160.5 (exo)	
220–410	37.80	330 (exo)	220–410	36.58	314 (exo)	Total decarboxylation

at 970–975 cm^{-1} reveals clearly the bridging bidentate nature of hydrazine ligands in both complexes [52–54]. The stretching frequencies in the region of 1625–1630 cm^{-1} is due to C=C functional group in fumarate ion. The asymmetric and symmetric stretching frequencies of carboxylate ions are seen in the region 1555–1550 cm^{-1} and 1385–1370 cm^{-1}, respectively with $\Delta\nu$ ($\nu_{as} - \nu_s$) separation of 180–170 cm^{-1}. This wide separation indicates monodentate linkage of both carboxylate groups in the dianion [32]. Thus, FTIR studies concluded that fumarate dianion coordinates to the metal as bidentate ligand via both carboxylate groups along with bridging bidentate hydrazine ligand.

3.2. Thermal decomposition studies

3.2.1. TG–DTG–DTA studies

Both $Co_xNi_{0.6-x}Zn_{0.4}Fe_2(C_4H_2O_4)_3{\cdot}6N_2H_4$ ($x = 0.1$ and 0.4) precursors exhibit similar decomposition behavior under dry atmosphere, as depicted in Figs. 2 and 3, respectively. Two step exothermic decomposition pathways can be inferred from the pattern, which includes dehydrazination as first exotherm which is followed by oxidative decarboxylation, indicating complete decomposition of precursors at 410 °C. The TG–DTG–DTA data of precursors is summarized in Table 2. The thermogravimtric analysis data show percent mass loss of 29.92% and 30.7% corresponding to $x = 0.1$ and $x = 0.4$ from RT to 220 °C. These values matches closely with theoretically calculated value for six hydrazine molecules in proposed formula and hence can be assigned for complete dehydrazination of precursors. However, initial mass loss of 6.76% and 7.12% can be assigned for removal of adsorbed hydrazine plus small amount moisture till 100 °C and thereafter, complete dehydrazination of precursors at 220 °C with 23.16% and 23.58% mass loss for $x = 0.1$ and $x = 0.4$, respectively. The differential thermal analysis (DTA) profile shows sharp exothermic peaks at 171.6 °C corresponding to dehydrazination of composition without any distinct peak for initial mass loss for $x = 0.1$, while for $x = 0.4$, small endotherm is observed initially at 74.5 °C due to loss of adsorbed hydrazine which is followed by exothermic peak due to total dehydrazination at 160.5 °C. The adsorbed hydrazine for $x = 0.4$ results in slight increase in hydrazine percentage and hence slight decrease in percentages of other metals with respect to theoretical ones (Table 2). In the second step of decomposition, major mass loss of 36.58–37.80% from 220 °C to 410 °C is attributed to oxidative decarboxylation of dehydrazinated precursors. Again, DTA shows more intense, sharp exothermic peaks of decarboxylation in these temperature ranges at 330 °C and 314 °C for $x = 0.1$ and 0.4, respectively. The DTG trace supports the observation of DTA trace. No peak in DTG indicates negligible mass loss beyond 410 °C. The total mass losses observed from TG traces and those obtained from total decomposition studies in air, were in agreement with theoretically calculated values considering assigned stoichiometry to the precursors.

3.2.2. Isothermal mass loss and hydrazine estimation

Based on TG–DTG–DTA results, isothermal mass loss studies were carried out on precursors at different set temperature in a programmable electric oven and simultaneously estimated for hydrazine loss. As can be seen from Table 3, the mass loss observed from room temperature to 70 °C is between 4.5–5% and can be considered for loss of hydrazine and adsorbed moisture. The simultaneous estimation of hydrazine content shows comparatively lower values for hydrazine loss i.e., about 3.0–3.5% and hence remaining loss at 70 °C corresponds to adsorbed moisture. When these precursors were heated to 100 °C and then to 125 °C, showed maximum loss of 13–14.5% altogether, corresponding to loss of 3.5–4 hydrazine molecules till 125 °C. Similarly hydrazine estimation supports above mass loss in this temperature zone. Further heating from 125 °C to 150 °C shows ~2 to 4% mass loss due to continuous dehydrazination. Finally beyond 150 °C, precursors catches fire but rarely undergo complete combustion as exothermicity of decomposition is lowered due to decrease in hydrazine content during each step of isothermal mass loss studies, thereby hindering the self propagating combustion. Hence, when ignited with burning splinter, the precursor decomposition process becomes continuous as presence of six hydrazine molecules together in precursor provides high enough exothermicity for the decomposition to be self propagating and autocatalytic.

3.3. Characterization of decomposed product

All the decomposed precursors were characterized by X-ray diffraction (XRD) spectroscopy and scanned in the region

Table 3
Isothermal mass loss, hydrazine content and total mass loss analysis data of $Co_xNi_{0.6-x}Zn_{0.4}Fe_2(C_4H_2O_4)_3{\cdot}6N_2H_4$ ($x = 0.1$ and 0.4).

Complexes x	Isothermal mass loss (%)/hydrazine content (%)					Total mass loss (%)	
	RT-70 °C	70–100 °C	100–125 °C	125–150 °C	Above 150 °C	Obs.	Calc.
0.1	4.50/24.20	2.64/21.80	10.40/11.38	2.20/9.30	Precursor decomposed	66.70	66.47
0.4	5.04/24.51	8.96/15.70	5.50/10.58	4.14/7.05	Precursor decomposed	67.50	66.47

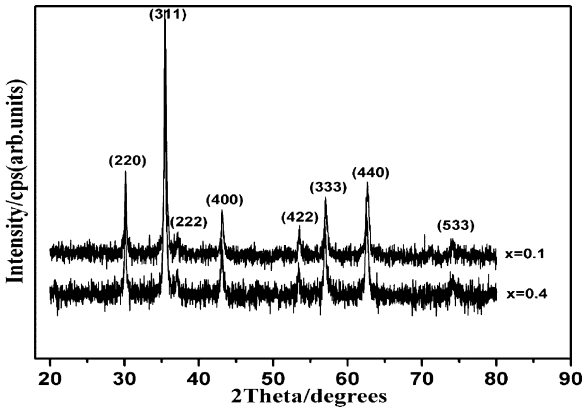

Fig. 4. XRD patterns of "as prepared" $Co_xNi_{0.6-x}Zn_{0.4}Fe_2O_4$ ($x = 0.1$ and 0.4).

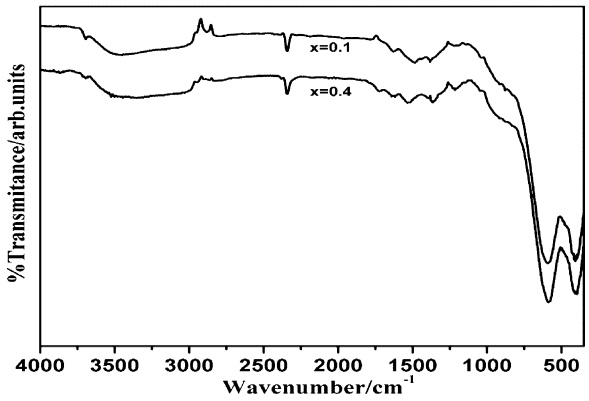

Fig. 6. FTIR spectra of "as prepared" $Co_xNi_{0.6-x}Zn_{0.4}Fe_2O_4$ ($x = 0.1$ and 0.4).

of 20–80°. The X- ray diffraction patterns confirm the formation of monophasic ferrite without any impurity phase as shown in Fig. 4. All the peaks are well resolved and indexed to cubic spinel ferrite system. The broadening of all reflection peaks indicates the small crystallite size. The average crystallite size was calculated by using full width at half-maximum (FWHM) of the diffraction peaks, according to the Scherrer's formula which was found to be in the range of 25–30 nm for both the samples. The morphology of samples was observed through TEM and electron diffraction (ED) pattern (Fig. 5) shows crystalline nature of the samples. The TEM shows particles with average diameter of 15–30 nm and are comparable to the average crystallite sizes of 25–30 nm calculated from XRD line broadening. In order to further confirm the phase purity of "as-prepared" ferrites, the autocatalytic decomposed products were also characterized by infrared spectroscopy in the region of 4000–400 cm^{-1}. As can be seen in the IR spectra of the samples (Fig. 6), the peaks between 575–595 cm^{-1} and 405–410 cm^{-1}, are characteristic peaks of ferrites and can be assigned to their tetrahedral and octahedral stretching vibrations [55,56].

Fig. 7 shows temperature dependence of normalized susceptibility χ_T/χ_{RT}, wherein variation of AC susceptibility with temperature shows the co-existence of single domain and superparamagnetic type of domain structure for both compositions [57]. The presence of broad maxima in the curves indicates the distribution of particle sizes in samples [58]. For $x = 0.1$, normalized susceptibility increases slowly with temperature up to the certain point called 'blocking temperature' and continuously decreases above blocking temperature attaining zero magnetization at Curie temperature ($T_c = 410\,°C$). The small and steady increase in susceptibility values and slow decrease with tailing indicates presence of superparamagnetic type domains as majority particles along with single domain particles [59]. For $x = 0.4$, majority of particles are single domain, which shows reasonably higher value increase in susceptibility with temperature and decreases in the same way as observe for $x = 0.1$ to attain Curie temperature ($T_c = 365\,°C$). The above observation is supported by TEM results, which shows comparatively smaller sized particles in $x = 0.1$ than $x = 0.4$.

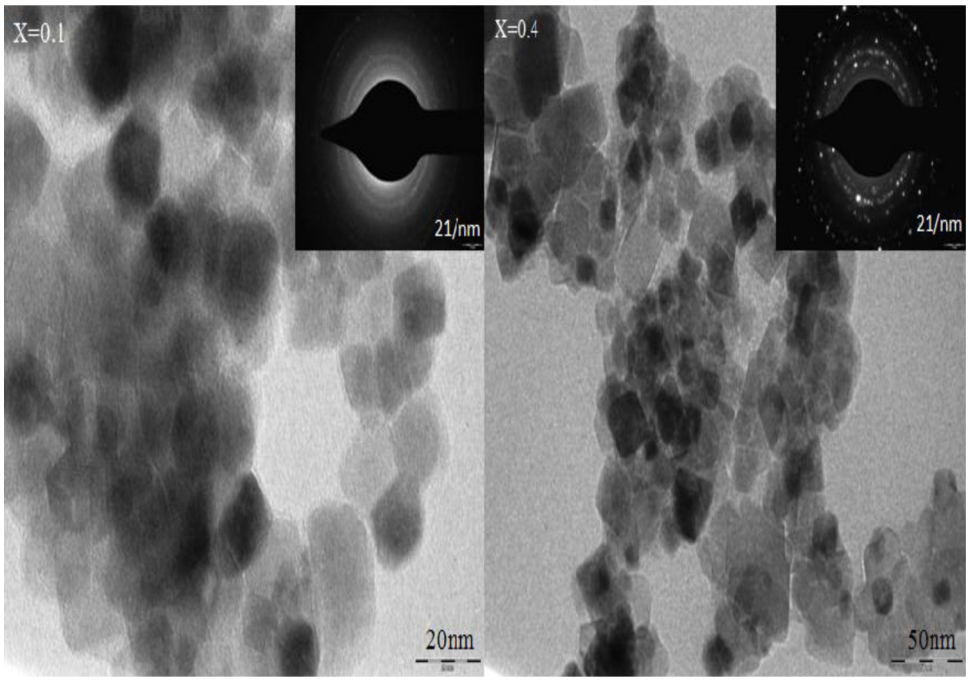

Fig. 5. TEM image and ED pattern of "as prepared" $Co_xNi_{0.6-x}Zn_{0.4}Fe_2O_4$ ($x = 0.1$ and 0.4).

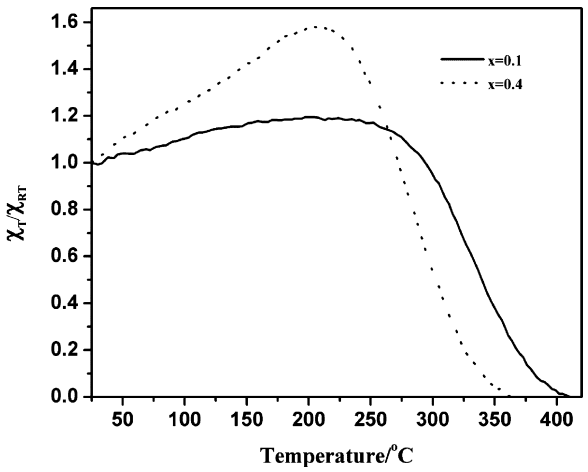

Fig. 7. Normalized susceptibility vs. temperature plot of "as prepared" $Co_xNi_{0.6-x}Zn_{0.4}Fe_2O_4$ ($x = 0.1$ and 0.4).

4. Conclusion

1. The hydrazinated nickel cobalt zinc ferrous fumarate, $Co_xNi_{0.6-x}Zn_{0.4}Fe_2(C_4H_2O_4)_3{\cdot}6N_2H_4$ ($x = 0.1$ and 0.4) can be prepared from sodium fumarate, metal chlorides and hydrazine hydrate in nitrogen atmosphere at room temperature.
2. The chemical analysis, infrared spectral analysis and thermal decomposition studies confirm the stoichiometry of precursor as $Co_xNi_{0.6-x}Zn_{0.4}Fe_2(C_4H_2O_4)_3{\cdot}6N_2H_4$ ($x = 0.1$ and 0.4). The thermal decomposition (TG–DTG–DTA) studies indicate two steps exothermic decomposition of precursors i.e., dehydrazination followed by oxidative decarboxylation which was proved to provide exothermicity sufficient enough for decomposition to be self propagating.
3. The XRD confirms the formation of single phase of "as prepared" $Co_xNi_{0.6-x}Zn_{0.4}Fe_2O_4$ ($x = 0.1$ and 0.4) which was also well supported by infrared spectroscopic studies. TEM images confirmed the nanosize nature of "as prepared" $Co_xNi_{0.6-x}Zn_{0.4}Fe_2O_4$ ($x = 0.1$ and 0.4) with particle size in the range of 15–30 nm.
4. AC susceptibility studies display along with T_c, the single domain-superparamagnetic type behavior by the small particles in both compositions.

Acknowledgements

Authors are grateful for the financial support from DST, New Delhi through the Nano Mission project, No. SR/NM/NS-86/2009 and also under FIST. The author S.G. Gawas is grateful to UGC, New Delhi for financial support under UGC-BSR fellowship, BSR F.4-12006 (BSR) 7-69-2007 (BSR). The authors are also thankful to Mr. Girish Prabhu, N.I.O. Goa for XRD facility and SAIF-IIT Bombay for recording TEM ED data.

References

[1] L.T. Lu, L.D. Tung, I. Robinson, D. Ung, B. Tan, J. Long, A.I. Cooper, D.G. Fernig, N.T. K. Thanh, Size and shape control for water-soluble magnetic cobalt nanoparticles using polymer ligands, J. Mater. Chem. 18 (2008) 2453–2458.
[2] S. Trudel, C.H.W. Jones, R.H. Hill, Magnetic properties of nanocrystalline iron oxide/amorphous manganese oxide nanocomposite thin films prepared via photochemical metal-organic deposition, J. Mater. Chem. 17 (2007) 2206–2218.
[3] S. Noor, M.A. Hakim, S.S. Sikder, S.M. Hoque, K.H. Maria, P. Nordlad, Magnetic behavior of Cd^{+2} substituted cobalt ferrites, J. Phys. Chem. Sol. 73 (2012) 227–231.
[4] D. Guo, X. Fan, G. Chai, C. Jiang, X. Li, D. Xue, Structural and magnetic properties of Ni Zn ferrite films with high saturation magnetization deposited by magnetron sputtering, Appl. Surf. Sci. 256 (2010) 2319–2322.
[5] L. Menini, M.C. Pereira, L.A. Parreira, J.D. Fabris, E.V. Gusevskaya, Cobalt and manganese substituted ferrites as efficient single-site heterogeneous catalysts for aerobic oxidation of monoterpenic alkenes under solvent-free conditions, J. Catal. 254 (2008) 355–364.
[6] F. Rajabi, N. Karimi, M.R. Saidi, A. Primo, R.S. Verma, R. Luque, Unprecedented selective oxidation of styrene derivatives using a supported iron oxide nanocatalyst in aqueous medium, Adv. Synth. Catal. 354 (2012) 1707–1711.
[7] U.B. Gawas, V.M.S. Verenkar, D.R. Patil, Nanostructured ferrite based electronic nose sensitive to ammonia at room temperature, Sens. Transducers 134 (11) (2011) 45–55.
[8] A.K. Gupta, M. Gupta, Synthesis and surface engineering of iron oxide nanoparticles for biomedical applications, Biomaterials 26 (2005) 3995–4021.
[9] K. Gheisari, S. Javadpour, H. Shokrollahi, B. Hashemi, Magnetic losses of the soft magnetic composites consisting of iron and Ni–Zn ferrite, J. Magn. Magn. Mater. 320 (2008) 1544–1548.
[10] A. Verma, T.C. Goel, R.G. Mendiratta, R.G. Gupta, High-resistivity nickel–zinc ferrites by the citrate precursor method, J. Magn. Magn. Mater. 192 (1999) 271–276.
[11] P. Priyadharsini, A. Pradeep, G. Chandrasekaran, Novel combustion route of synthesis and characterization of nanocrystalline mixed ferrites of Ni–Zn, J. Magn. Magn. Mater. 321 (2009) 1898–1903.
[12] J. Azadmanjiri, Structural and electromagnetic properties of Ni–Zn ferrites prepared by sol–gel combustion method, Mater. Chem. Phys. 109 (2008) 109–112.
[13] Z. Yue, J. Zhou, L. Li, Z. Gui, Effects of MnO_2 on the electromagnetic properties of Ni–Cu–Zn ferrites prepared by sol–gel auto-combustion, J. Magn. Magn. Mater. 233 (2001) 224–229.
[14] D.H. Bobade, S.M. Rathod, M.L. Mane, Sol–gel auto-combustion synthesis, structural and enhanced magnetic properties of Ni^{2+} substituted nanocrystalline Mg–Zn spinel ferrite, Phys. B 407 (2012) 3700–3704.
[15] G.A. El-Shobakya, A.M. Turky, N.Y. Mostafa, S.K. Mohamed, Effect of preparation conditions on physicochemical, surface and catalytic properties of cobalt ferrite prepared by coprecipitation, J. Alloys Compd. 493 (2010) 415–422.
[16] A. Xia, C. Jin, D. Du, Y. Sun, L. Tong, Effects of impurity Na^+ ions on the structural and magnetic properties of Ni–Zn–Cu ferrite powders: an improvement for chemical coprecipitation method, J. Magn. Magn. Mater. 323 (2011) 2080–2082.
[17] T. Kagotani, R. Kobayasha, S. Sugimoto, K. Inomata, K. Okayama, J. Akedo, Magnetic properties and microwave characteristics of Ni–Zn–Cu ferrite film fabricated by aerosol deposition method, J. Magn. Magn. Mater. 290–291 (2005) 1442–1445.
[18] S.L. Pereira, H.D. Pfannes, A.A. Mendes Filhob, L.C.B. de Miranda Pinto, M.A. Chíncaro, A comparative study of Ni–Zn ferrites modified by the addition of cobalt, Mater. Res. 2 (3) (1999) 231–234.
[19] S. Thakur, S.C. Katyal, A. Gupta, V.R. Reddy, S.K. Sharma, M. Knobel, M. Singh, Nickel–zinc ferrite from reverse micelle process: structural and magnetic properties Mossbauer spectroscopy characterization, J. Phys. Chem. C 113 (2009) 20785–20794.
[20] R.D.K. Misra, S. Gubbala, A. Kale, W.F. Egelhoff Jr., A comparison of the magnetic characteristics of nanocrystalline nickel, zinc and manganese ferrites synthesized by reverse micelle technique, Mater. Sci. Eng. B 111 (2004) 164–174.
[21] A. Verma, T.C. Goel, R.G. Mendiratta, P. Kishan, Magnetic properties of nickel zinc ferrites prepared by the citrate precursor method, J. Magn. Magn. Mater. 208 (1) (2000) 13–19.
[22] O. Carp, L. Patron, G. Pascu, I. Mindru, N. Stanica, Thermal investigations of nickel–zinc ferrites formation from malate coordination compounds, J. Therm. Anal. Calorim. 84 (2) (2006) 391–394.
[23] N.D. Chaudhari, R.C. Kambale, D.N. Bhosale, S.S. Suryavanshi, S.R. Sawant, Thermal hysteresis and domain states in Ni–Zn ferrites synthesized by oxalate precursor method, J. Magn. Magn. Mater. 322 (2010) 1999–2005.
[24] D.N. Bhosale, V.M.S. Verenkar, K.S. Rane, P.P. Bakare, S.R. Sawant, Initial susceptibility studies on Cu–Mg–Zn ferrites, Mater. Chem. Phys. 59 (1) (1999) 57–62.
[25] B.N. Sivasankar, S. Govindarajan, Hydrazine mixed metal malonates – new precursors for metal cobaltites, Mater. Res. Bull. 31 (1) (1996) 47–54.
[26] K.S. Rane, H. Uskaikar, R. Pednekar, R. Mhalsikar, The low temperature synthesis of metal oxides by novel hydrazine method, J. Therm. Anal. Calorim. 90 (3) (2007) 627–638.
[27] M.M.A. Sekar, K.C. Patil, Hydrazine carboxylate precursors to fine titania, zirconia and zirconium titanate, Mater. Res. Bull. 28 (1983) 485–492.
[28] D. Gajapathy, K.C. Patil, V.R. Pai Vernekar, Low temperature ferrite formation using metal oxalate hydrazinate precursor, Mater. Res. Bull. 17 (1) (1982) 29–32.
[29] K.C. Patil, Metal hydrazine complexes as precursor to oxide materials, Proc. Ind. Acad. Sci. 96 (6) (1986) 459–464.
[30] D. Gajapathy, K.C. Patil, K. Kishore, Thermal reactivity of metal oxalate hydrazinates, Thermochim. Acta 52 (1982) 113–120.
[31] B.N. Sivasankar, S. Govindrajan, Acetate and malonate complexes of cobalt(II), nickel(II) and zinc(II) with hydrazinium cation: preparation, spectral and thermal studies, J. Therm. Anal. 48 (6) (1997) 1401–1413.

[32] B.N. Sivasankar, Cobalt(II), nickel(II) and zinc(II) dicarboxylate complexes with hydrazine as bridged ligand: characterization and thermal degradation, J. Therm. Anal. Calorim. 86 (2) (2006) 385–392.
[33] S.Y. Sawant, V.M.S. Verenkar, S.C. Mojumdar, Preparation, thermal, XRD, chemical and FTIR spectral analysis of $NiMn_2O_4$ nanoparticles and respective precursor, J. Therm. Anal. Calorim. 90 (3) (2007) 669–672.
[34] R.A. Porob, S.Z. Khan, S.C. Mojumdar, V.M.S. Verenkar, Synthesis, TG, DSC and spectral study of $NiMn_2(C_4H_4O_4)_3{\cdot}N_2H_4$ a precursor for $NiMn_2O_4$ nanoparticles, J. Therm. Anal. Calorim. 86 (3) (2006) 605–608.
[35] P. Ravindranathan, K.C. Patil, Thermal reactivity of metal formate hydrazinates, Thermochim. Acta 71 (1983) 53–57.
[36] G.V. Mahesh, K.C. Patil, Thermal reactivity of metal acetate hydrazinates, Thermochim. Acta 99 (1) (1986) 153–158.
[37] K.S. Rane, V.M.S. Verenkar, Synthesis of ferrite grade g-Fe_2O_3, Bull. Mater. Sci. 24 (1) (2001) 39–45.
[38] L.R. Gonsalves, V.M.S. Verenkar, S.C. Mojumdar, Preparation and characterization of $Co_{0.5}Zn_{0.5}Fe_2(C_4H_2O_4)_3{\cdot}6N_2H_4$, J. Therm. Anal. Calorim. 96 (1) (2009) 53–57.
[39] L.R. Gonsalves, S.C. Mojumdar, V.M.S. Verenkar, Synthesis of cobalt nickel ferrite nanoparticles via autocatalytic decomposition of the precursor, J. Therm. Anal. Calorim. 100 (3) (2010) 789–792.
[40] U.B. Gawas, V.M.S. Verenkar, Synthesis, thermal and infrared spectroscopic studies of hydrazinated mixed metal fumarates, J. Therm. Anal. Calorim. 115 (1) (2014) 375–381.
[41] U.B. Gawas, V.M.S. Verenkar, S.C. Mojumdar, Synthesis and characterization of $Ni_{0.6}Zn_{0.4}Fe_2O_4$ nano-particles obtained by auto catalytic thermal decomposition of carboxylato–hydrazinate complex, J. Therm. Anal. Calorim. 104 (3) (2011) 879–883.
[42] U.B. Gawas, S.C. Mojumdar, V.M.S. Verenkar, Synthesis, characterization, infrared studies and thermal analysis of $Mn_{0.6}Zn_{0.4}Fe_2(C_4H_2O_4)_3{\cdot}6N_2H_4$ and its decomposition product $Mn_{0.6}Zn_{0.4}Fe_2O_4$, J. Therm. Anal. Calorim. 100 (3) (2010) 867–871.
[43] U.B. Gawas, S.C. Mojumdar, V.M.S. Verenkar, $Ni_{0.5}Mn_{0.1}Zn_{0.4}Fe_2(C_4H_2O_4)_3{\cdot}6N_2H_4$ precursor and $Ni_{0.5}Mn_{0.1}Zn_{0.4}Fe_2O_4$ nanoparticles. Preparation, IR, spectral, XRD, SEM-EDS and thermal analysis, J. Therm. Anal. Calorim. 96 (1) (2009) 49–52.
[44] L.R. Gonsalves, S.C. Mojumdar, V.M.S. Verenkar, Synthesis and characterization of ultrafine spinel ferrite obtained by precursor combustion technique, J. Therm. Anal. Calorim. 108 (3) (2012) 859–863.
[45] U.B. Gawas, V.M.S. Verenkar, S.C. Mojumdar, Nano-crystalline $Mn_{0.3}Ni_{0.3}Zn_{0.4}Fe_2O_4$ obtained by novel fumarato-hydrazinate precursor method – synthesis, characterization and studies of magnetic and electrical properties, J. Therm. Anal. Calorim. 108 (3) (2012) 865–870.
[46] L.R. Gonsalves, V.M.S. Verenkar, Synthesis and thermal studies of the cobalt zinc ferrous fumarato-hydrazinate – a precursor to obtain nanosize ferrites, J. Therm. Anal. Calorim. 108 (3) (2012) 871–875.
[47] L.R. Gonsalves, V.M.S. Verenkar, Synthesis and characterization of nanosized nickel-doped cobalt ferrite obtained by precursor combustion method, J. Therm. Anal. Calorim. 108 (3) (2012) 877–880.
[48] U.B. Gawas, V.M.S. Verenkar, Synthesis, thermo-analytical and IR spectral studies of hydrazinated mixed metal carboxylates: a single source precursor to nanosize mixed metal oxides, Thermochim. Acta 556 (2013) 41–46.
[49] U.B. Gawas, V.M.S. Verenkar, Synthesis, thermal and infrared spectroscopic studies of hydrazinated mixed metal fumarates, J. Therm. Anal. Calorim. 115 (2014) 375–381.
[50] G.H. Jeffery, J. Bassett, J. Mendham, R.C. Denney, Vogel's Textbook of Quantitative Inorganic Analysis, fifth ed., Longman, England, 1989.
[51] D.H. Wilkins, The determination of nickel, cobalt, iron and zinc in ferrites, Anal. Chim. Acta 20 (1959) 271.
[52] B.T. Heaton, C. Jacob, P. Page, Transition metal complexes containing hydrazine and substituted hydrazines, Coord. Chem. Rev. 154 (1996) 193.
[53] T. Premkumar, S. Govindarajan, The chemistry of hydrazine derivative-thermal behavior and characterisation of hydrazinium salts and metal hydrazine complexes of derivatives of 4,5-imidazoledicarboxylic acid, Thermochim. Acta 386 (2002) 35.
[54] S. Vairan, T. Premkumar, S. Govindarajan, Preparation and thermal behaviour of divalent transition metal complexes of pyromellitic acid with hydrazine, J. Therm. Anal. Calorim. 101 (2010) 979.
[55] R.D. Waldron, Infrared spectra of ferrites, Phys. Rev. 99 (1955) 1727–1735.
[56] I. Sharifi, H. Shokrollahi, Nanostructural, magnetic and Mossbauer studies of nanosized $Co_{1-x}Zn_xFe_2O_4$ synthesized by co-precipitation, J. Magn. Magn. Mater. 324 (2012) 2397–2403.
[57] P. Yaseneva, M. Bowker, G. Hutchings, Structural and magnetic properties of Zn-substituted cobalt ferrites prepared by co-precipitation method, Phys. Chem. Chem. Phys. 13 (2011) 18609–18614.
[58] R. Iyer, R. Desai, R.V. Upadhyay, Low temperature synthesis of nanosized Mn_{1-x} Zn_x Fe_2O_4 ferrites and their characterizations, Bull. Mater. Sci. 32 (2) (2009) 141–147.
[59] B.P. Ladgaonkar, P.N. Vasambekar, A.S. Vaingankar, Effect of Zn^{+2} and Nd^{+3} substitution on magnetization and AC susceptibility of Mg Ferrite, J. Magn. Magn. Mater. 210 (2000) 289–294.